Dipole Orientation and Surface Cluster Size Effects on Chemisorption-Induced Magnetism: A DFT Study of the Interaction of Gold−Thiopolypeptide

Luis Puerta,*,† Héctor J. Franco,‡ Juan Murgich,§ Carlos Gonzalez,|| Yamil Simón-Manso,|| and Vladimiro Mujica*,‡,⊥,#

Departamento de Química, FACYT, Universidad de Carabobo, Apartado 2005, Valencia, Edo. Carabobo, Venezuela, Escuela de Química, Universidad Central de Venezuela, Apartado 47102, Caracas 1041-A, Venezuela, Centro de Química, IVIC, Apartado 21827, Caracas 1020A, Venezuela, Physical and Chemical Properties Division, Building 221, Room A111, NIST, Gaithersburg, Maryland 20899, Department of Chemistry, Northwestern University, 2145 Sheridan Road, Evanston, Illinois 60208-3113, and Center for Nanoscale Materials, Argonne National Laboratory, Argonne, Illinois 60439-4831

Received: November 9, 2007; Revised Manuscript Received: June 27, 2008

A nanosystem formed by a high electric dipole moment thiopolypeptide α-helix, consisting of eight L-glycine units, chemisorbed on the (111) surface of Au_{23} and Au_{55} clusters, with the S as the linking atom, was studied using the wave function broken symmetry UDFT method. We have found a strong correlation between the orientation of the electric dipole of the α-helix and charge transfer and the magnetic behavior of the adsorbate−cluster system. Upon chemisorption, dipole moments may be quenched or enhanced, with respect to the gas phase value, with the strongest reduction corresponding to the magnetic state. A reduction of the α-helix's electric dipole with the net charge transfer from the Au surface was obtained for the more stable state. In this state description, it may happen that the calculated spin densities of the chemisorbed α-helix and its free radical form are similar. The magnetic properties are strongly dependent on the size of the Au cluster and on its electronic structure with respect to nuclei positions. In general, the localized spin density per atom increases and the magnetization of the extended system decreases with cluster size, a trend found experimentally for organic monolayers with a similar type of adsorbate we consider here.

Introduction

Recent experiments have confirmed that functionalized gold nanoparticles and films of organic molecules on gold surfaces have complex magnetic behavior in sharp contrast to the fact that both gold and organic ligands are non magnetic.[1] The tendency toward magnetism is determined by a competition between electronic exchange and kinetic energy effects. Whereas the parallel alignment of the electronic spin leads to a gain of exchange energy, it also causes a loss of kinetic energy. Most solid-state systems are nonmagnetic, since the gain in exchange is dominated by the loss in the kinetic energy. Only if the electrons are sufficiently localized, magnetism occurs as, for instance, in metals such as Fe, Co, Ni, and Cr. The tendency toward magnetism is enhanced in lower-dimensional systems like metallic surfaces and interfaces, multilayers, ultrathin films and wires, and magnetic clusters deposited on surfaces.[2]

The formation of chemisorption-induced magnetism has been reported experimentally, with magnetizations ranging from 0.0036 μ_b for thiolate-capped Au nanoparticles,[3] 0.05−1 μ_b[4] for alkanethiol self-assembled monolayers, and up to tens of Bohr magnetons per adsorbed molecule in monolayers of polyalanine polypeptides on Au substrates.[5] Using finite perturbation theory, Gonzalez et al.[1] have explained the origin of the observed magnetism in Au (cluster)−ligand systems with different chemical linkers and provided a theoretical explanation of the experimental observation that S-linked ligands induce magnetism in Au, whereas using N as a linker does not affect the diamagnetic behavior of Au.[1]

Namaan et al.[5−7] studied systems that showed unusual magnetic properties in self-assembled layers of polypeptides with high dipole moment (>50 D) chemisorbed on Au surfaces. They have suggested[8−10] that an electronic density rearrangement in the adsorbed molecules is produced by their chemisorption on the metal surface.[6] The origin of such rearrangement may be attributed to a charge transfer process between the metallic surface and the organic substrate that induces an appreciable electric dipole moment reduction in the adsorbed molecules and their intermolecular repulsion. The electrons transferred to/from the substrate may lead to the occupation of low energy states associated with the magnetic properties observed in these systems.[7]

In principle, multireference methods such as CASSCF are required to describe rigorously the ferromagnetically or antiferromagnetically coupled spin states. In practice, Noodleman's broken symmetry (BS) approach,[11−16] which makes use of the Heisenberg spin operator formalism to obtain a reasonable electronic structure description, has provided a working protocol for single-reference methods, such as DFT, employing the unrestricted spin formalism. The BS approach has been employed with considerable success to interpret the magnetic and spectroscopic properties of a variety of biologically active species.[17] Density functional theory (DFT) calculations have proved to be a powerful tool to describe the magnetism of itinerant electrons in solids.[2] Such calculations are not only the

* To whom the correspondence should be addressed. E-mail: lpuerta@uc.edu.ve (L.P.), vmujica@chem.northwestern.edu (V.M.).
† Universidad de Carabobo.
‡ Universidad Central de Venezuela.
§ IVIC.
|| NIST.
⊥ Northwestern University.
Argonne National Laboratory.

10.1021/jp710748h CCC: $40.75 © 2008 American Chemical Society
Published on Web 09/13/2008

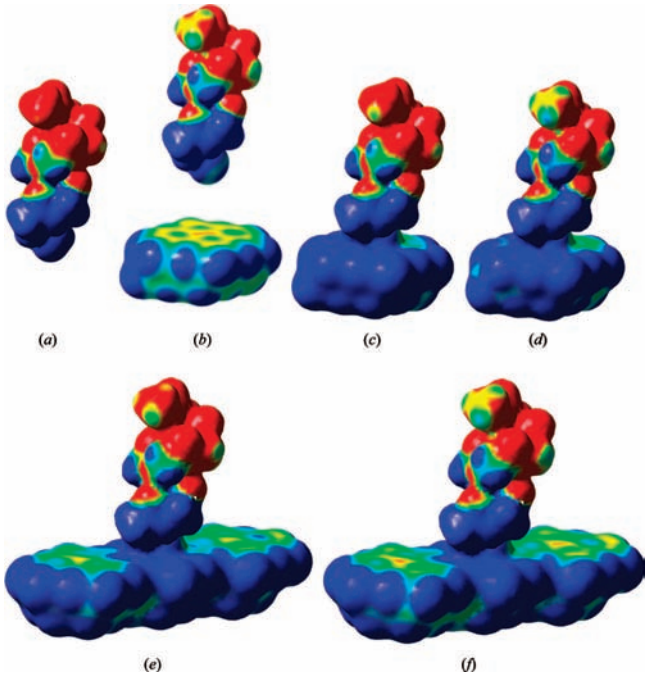

Figure 1. Electrostatic potential mapped over the electronic isodensity surface set at 0.002 (e/Å^3) (red = −8.79 kcal/mol, deep blue = 11.30 kcal/mol). (a) Free mercapto-α-helix of eight L-glycine units polypeptide molecule as shown in Figure 3 at its singlet ground state [μ = 31.0 (μ_{EBS} = 33.4) D]. (b) Free thio-α-helix radical (μ = 19.0 D) and free plain Au_{23} cluster radical [μ = 0.2 (μ_{EBS} = 0.1) D]. (c) Thio-α-helix chemically adsorbed on the (111) plane of Au_{23} cluster at its singlet state (μ = 26.1 D) under the down+ conformation, as also shown in Figure 4b. (d) Ditto when the nanosystem is found at its magnetic state (μ = 22.4 D). (e) Thio-α-helix chemically adsorbed on the (111) plane of Au_{55} cluster at its singlet state (μ = 21.7 D) under the down+ conformation, as also shown in Figure 4c. (f) Ditto when the nanosystem is found at its magnetic state (μ = 16.2 D). By simple inspection of the drawings, the variation of electrostatic potential at the thio-α-helix's top, tracked by the methyl group, is evident.

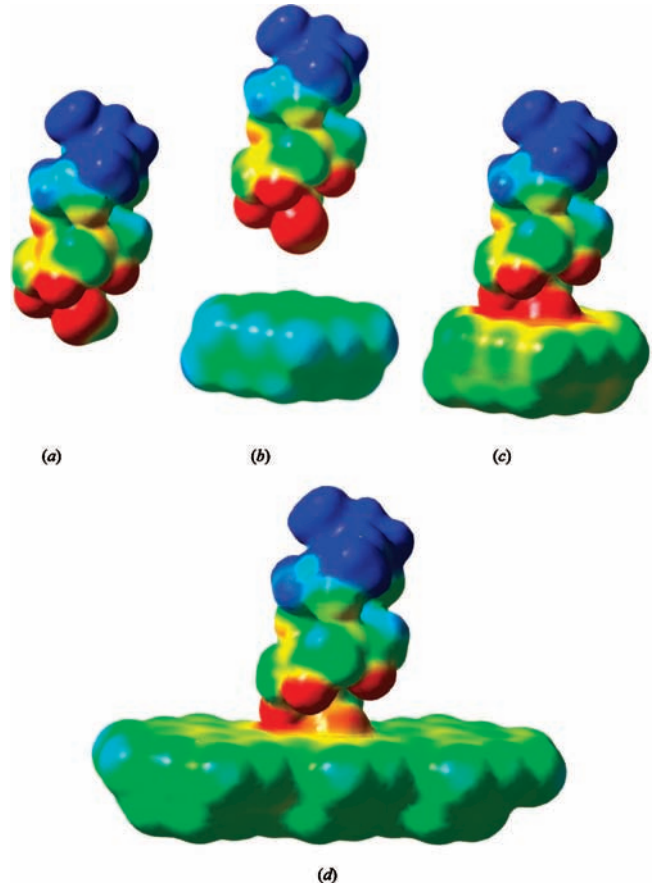

Figure 2. Electrostatic potential mapped over the electronic isodensity surface set at 0.002 (e/Å^3) (red = −43.93 kcal/mol, deep blue = 37.65 kcal/mol) (a) Free mercapto-α-helix of eight L-glycine units thiopolypeptide molecule at its singlet ground state [μ = 31.0 (μ_{EBS} = 34.5) D]. (b) Free thio-α-helix radical (μ = 31.2 D) and free plain Au_{23} cluster radical [μ = 0.2 (μ_{EBS} = 0.1) D]. (c) Thio-α-helix chemically adsorbed on the (111) plane of Au_{23} cluster under the up+ conformation on the Au_{23} cluster at its singlet state (μ = 38.9 D) as also shown in Figure 6b. When found at its magnetic state (μ = 38.9 D) no relative significant potential changes are observed, so a practically identical mapped surface to that shown in c, is found. (d) Ditto on the Au_{55} cluster, as also shown in Figure 6c (μ = 37.1 D). By inspecting the drawings, the variation of potential at the thio-α-helix's middle and lower sections tracked by the three front methylene groups is evident. The main changes in potential are observed at the middle light blue shaded methylene group, at the lower green shaded methylene group, and at the sulfur atom, all shifting toward blue color.

basis for quantitative theoretical determination of spin magnetic moments but can also be used to understand the basic mechanisms that lead to the occurrence of magnetism in some solids.

We are interested in nanosystems that model those studied by Naaman et al. Our goal is to study their electronic structure and magnetic properties and verify some of the hypothesis used in the interpretation of the experimental data.[8−10] We represent the chemisorbed thiopolypeptide layer on an Au surface with a single α-helix molecule of high electric dipole moment linked to the model surface (111) of Au clusters via a S atom. The S atom was located in a position that was between the face-centered cubic hole and a bridge.[18] The effect of changing the orientation of the polypeptide electric dipole moment and of the Au cluster size on the magnetic and electrical properties was explored for this system. The spin density and charge distribution localized in the chemisorbed thiopolypeptide molecule was studied using the DFT with the BS approach. The density of states (DOS) near the Fermi level was also calculated for the different Au clusters.

Calculation

We have studied the spin and charge distributions in a Au (cluster)−ligand system, which is intended to model a nanosystem formed after the chemisorption of a mercapto-α-helix polypeptide of eight L-glycine units (−HNCOCH$_2$−) with a high electric dipole moment (∼30 D) (Figures 3 and 7) to a gold surface. To this end we have chosen the (111) plane of Au to construct the Au_{23} and Au_{55} clusters, whose geometry corresponds to a face-centered cubic phase (Figures 4b,c and 6b,c). The (111) Au surfaces contained just two layers; for the A_{23} cluster, the upper one was formed with 14 Au atoms and the lower by 9. For the Au_{55} cluster, the upper layer was formed with 34 Au atoms and the lower layer with 21. Two configurations of the systems were used: one with the negative (up+) tip of the electric dipole of the helix pointing nearly perpendicularly to the (111) plane (∼85°) and another one with the inverted configuration (down+). We have adopted the same notation as Ray et al.[19] for the dipole moment in Au surfaces. In the down+ configuration, the positive polypeptide carbonyl group is bonded to the CH_2SH group and the positive tip of the dipole is oriented toward the metallic surface. For the up+ configuration, the amine group (N-terminal) is bonded to the CH_2SH group with the negative tip near the metal surface. In both configurations, the −CH_2S− group is covalently bonded

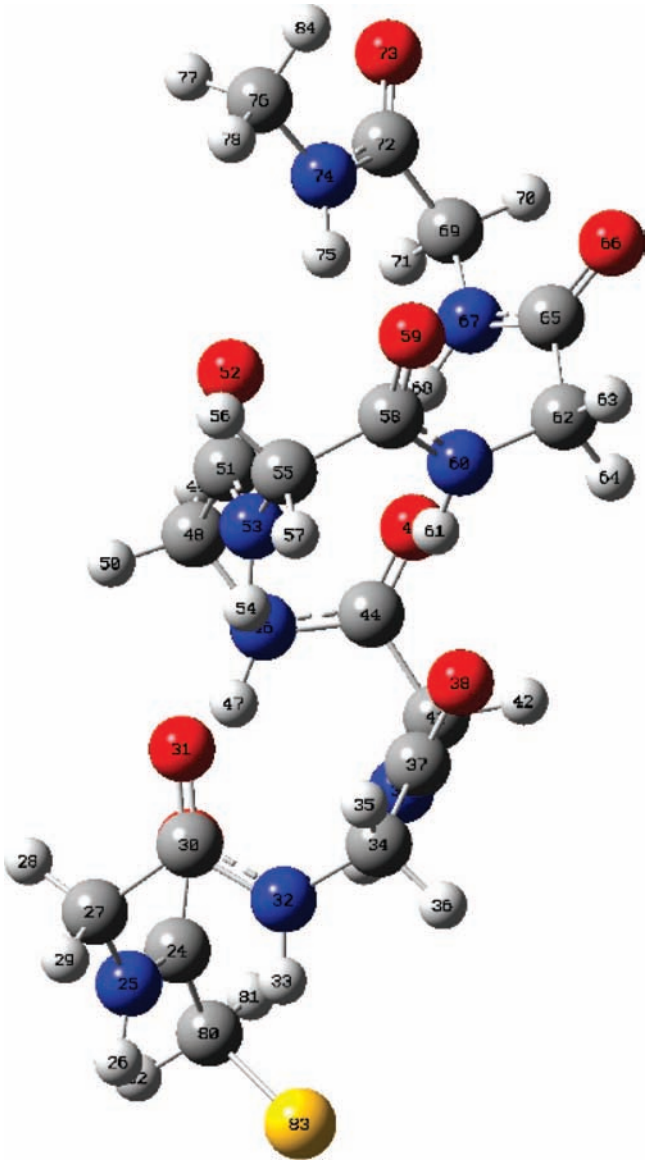

Figure 3. Drawing of down+ thio-α-helix radical showing its labeled atoms. Nitrogen atom 39 (blue) is eclipsed by carbon atom 37 (gray) at the third position away from sulfur atom 83 (yellow). Red spheres represent oxygen atoms.

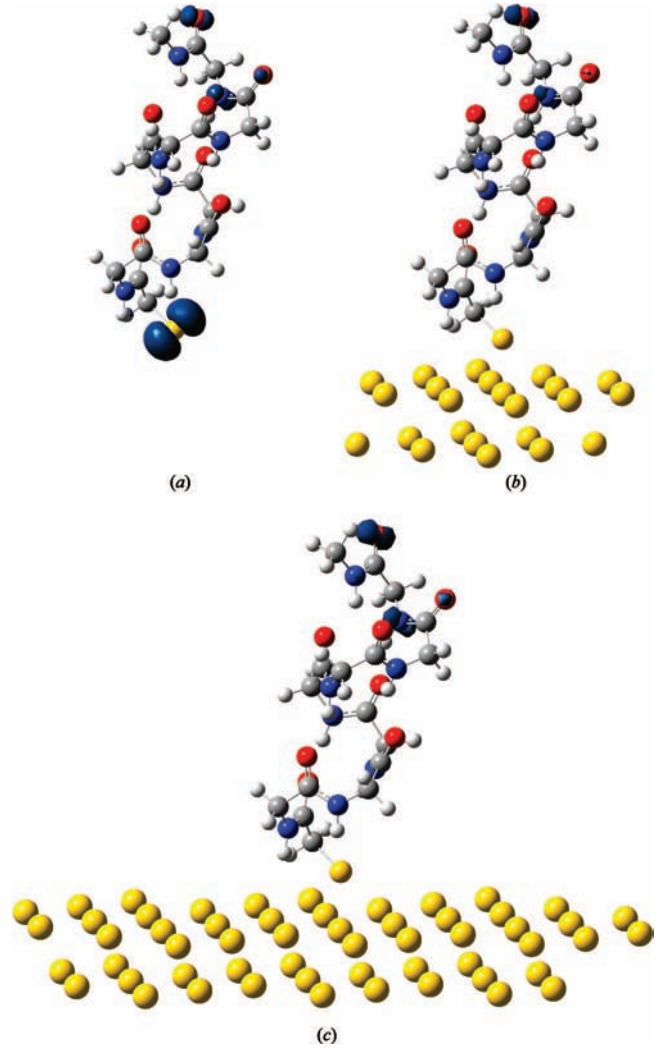

Figure 4. (a) Thio-α-helix free radical for the spin isovalue = 5.0 × 10^{-3} (au). (b) Ditto on the Au_{23} cluster. (c) Ditto on the Au_{55} cluster.

to the metallic surface through the S atom. The nanosystems were built and optimized using molecular mechanics (MM) with a MM+ force field.[20,21] The lower energy conformations were found by fixing the S and Au atoms to known positions,[18] keeping fixed the secondary structure of all L-glycine units and applying conventional MM optimization procedures.[20] Single-point unrestricted density functional theory (UDFT) calculations were performed for finding the regular singlet state (nonspin broken symmetry) for the nanosystem, its fragments, and the mercapto-α-helix derivatives. The more stable magnetic states were found using the hybrid UPBE1PBE DFT functional with the LANL2 pseudopotential.[22] The LanL2MB basis set for the Au atoms and a 3-21G* set for the light elements were used in the calculation.[22] For both configurations of the Au_{23} nanosystem, their fragments and mercapto-α-helix calculations were also conducted using the extended basis set LanL2DZ (double-ζ) with the additional basis sets 6d and 10f. No calculations of this sort were performed for the Au_{55} nanosystems, since it was practically impossible to use full-electron extended basis sets for such large systems. The use of the extended basis set was mostly intended to validate the use of the smaller set. We found that indeed the qualitative trends for both basis sets are similar.

The magnetic states (antiferromagnetic ones) were found with the wave function BS-UDFT method.[12,14,15,23−25] Isospin, and isoelectron density plots were obtained using Gaussian 03M[22] and GaussViewM.[26] Additionally, the HOMO and LUMO plots were also calculated for several singlet states (Figure 7), as well as the SOMO α, SOMO β, and SOMO $\beta-1$ plots for the magnetic states (Figure 8). Electrostatic potential maps were calculated over the 0.002 e/Å^3 isoelectronic density surfaces (Figures 1 and 2).

The relative stability between the magnetic and the singlet states for the studied nanosystems, defined as $\Delta E = E_{\text{magnetic}} - E_{\text{singlet}}$, where E_{magnetic} is the total energy of the magnetic state and E_{singlet} is that of the singlet state, was calculated. Also, the electric charges for the S-α-helix and the cluster, both isolated and forming the nanosystem, were calculated for the magnetic (M) and singlet (S) states ($q_{\text{thio-α(M)}}$ and $q_{\text{thio-α(S)}}$) employing the sum of its atomic NBO and Mullliken charges.[22] The charge difference between the magnetic and singlet states ($\Delta Q_{\text{thio-α}} = q_{\text{thio-α(M)}} - q_{\text{thio-α(S)}}$), the S-α-helix Mulliken spin population $S_{\text{thio-α}}$, the magnetic moments μ_s, and the electric dipole μ moments were also determined. The total NBO and Mulliken charges for the plain α-helix q_α and both Au_{23} and Au_{55} clusters,

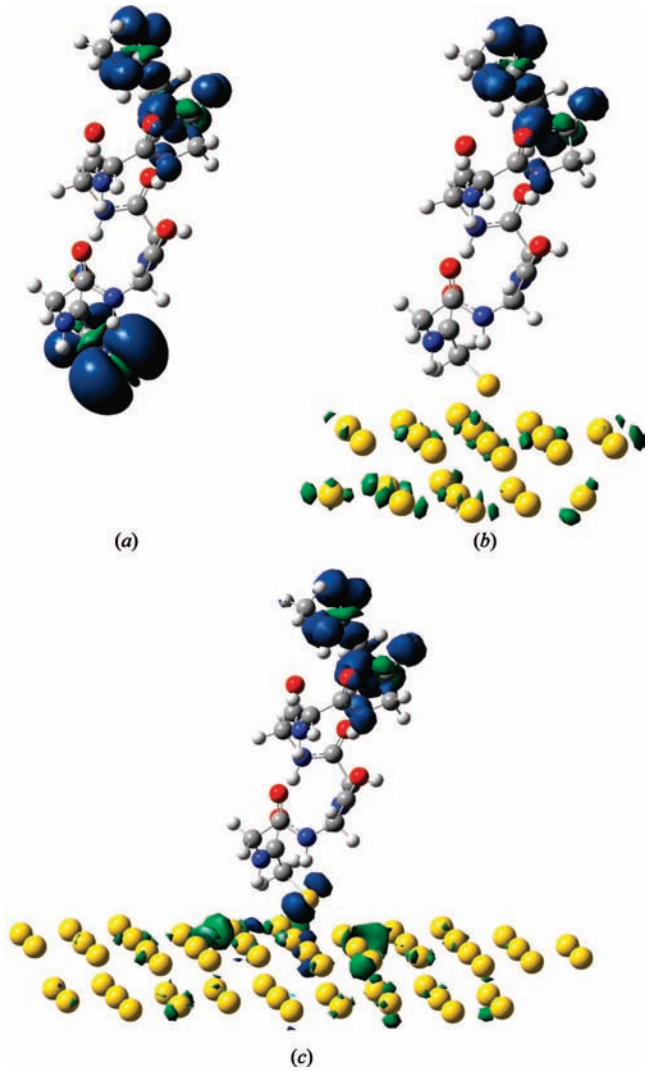

Figure 5. (a) Thio-α-helix free radical for the spin isovalue = 4.0×10^{-4} (au). (b) Ditto on the Au_{23} cluster. (c) Ditto on the Au_{55} cluster. Blue and green surfaces display net positive and negative spin densities, respectively.

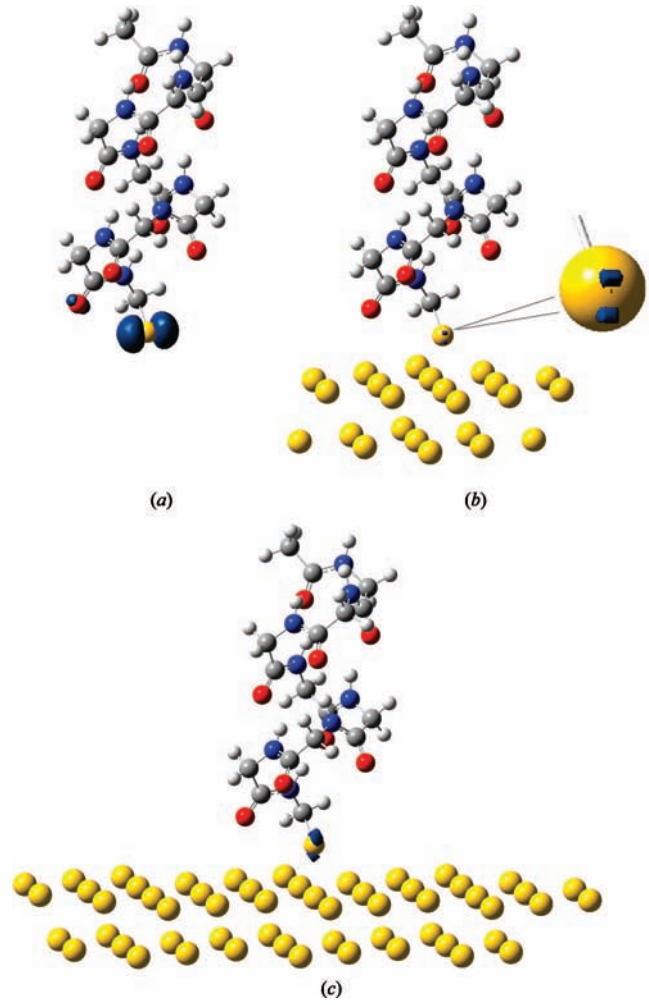

Figure 6. (a) up+ conformation thio-α-helix free radical for the spin isovalue = 1.0×10^{-2} (au). (b) Ditto on the Au_{23} cluster at isovalue = 1.0×10^{-8} (au). (c) Ditto on the Au_{55} cluster. Note the enlarged drawing of the bridging S atom showing its tiny localized spin density in part b. Blue and green surfaces show net positive and negative spin densities, respectively.

q_{Au}, were also obtained. The magnetic moment was evaluated following two methods. The first one was using the $\langle S^2 \rangle$ value with Gaussian 03M.[22] This calculation was done without taking into account the annihilation of the excited states. We considered the electronic correlation effect and the contribution of the excited states in the description of the magnetic state.[27] The second method was using natural population analysis (NPA) instead of the usual Mulliken one for obtaining the spin populations on each atom[28]and then we got $\mu_{S\text{-}NPA}$. We also evaluated the energy splitting ΔE_{ss} as the SOMO α − SOMO β energy difference.[29]

To mimic the continuous DOS characteristic of an extended system, we construct a Gaussian distribution around each energy eigenvalue of the cluster to generate an approximation to the DOS of the surface. An algorithm using Spline was implemented for the required interpolations.[30] The total DOS was evaluated as α SDOS + β SDOS using a line width for the Gaussian curves of 0.1 eV.[31] The spin asymmetry was defined as the difference α SDOS − β SDOS. In the algorithm, we made two approximations to evaluate the net magnetic spin states number to obtain the nanosystem magnetic moment. In the first one, we obtained $\mu_s(0.0)$ from the area below the curve α SDOS − β SDOS integrated from −31.0 eV up to the Fermi level set at the HOMO,[32] also set at 0.0 eV and, in the second one, we followed the same procedure, but integration was evaluated up to the $\Delta E_{ss}/2$ eV value[33,34] to give $\mu_s(\Delta E_{ss}/2)$. Our method for estimating the bulk value of the magnetic moment (μ_s) was first tested against experimental results for bulk Fe.[28] Such procedure consisted of first doing a calculation for a two-atom Fe cluster and, then, finding a calibrating factor once the net magnetic spin states number was evaluated. All (S)DOS spectra were plotted as functions of energy within the (−31.0, 4.0) eV energy interval. All reported calculations were done at the self-consistent field (SCF) convergence criterion of 10^{-8}.[22]

Contrary to the down+ configuration case for the Au_{23} cluster nanosystem, we found serious difficulty in finding a magnetic state when the convergence criterion was set to 10^{-8} for the larger cluster. The 10^{-5} convergence criterion was our limit before we had to start using techniques for obtaining convergence. To obtain higher convergence values, it was necessary to use the "vshift" technique.[22] With a vshift value of 5 millihartrees, a convergence of 10^{-8} was obtained for the UDFT-SCF calculation. The results were such that it corresponded to a state at approximately 16 cal/mol below the state found using the convergence criterion of 10^{-5}.

The results of variations in the atomic charges were dependent on the model used to analyze them. For some configurations,

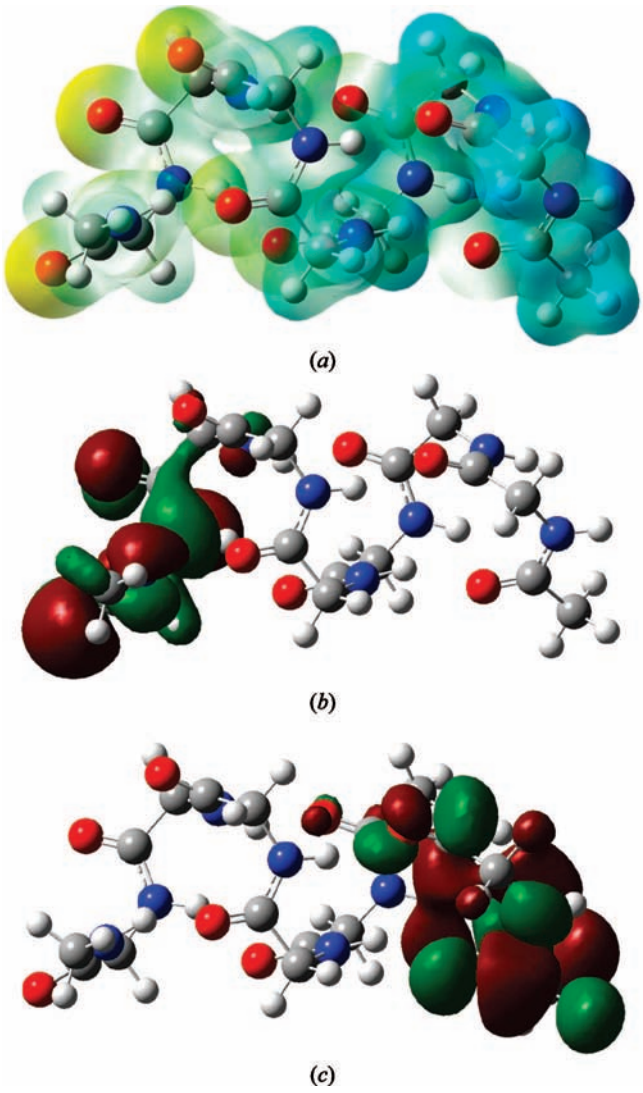

Figure 7. (a) Electrostatic potential mapped over the electronic isodensity surface (yellow = −92.24 kcal/mol, deep blue = 184.49 kcal/mol) (b) HOMO at the negative end tip of the α-helix molecule. (c) LUMO at the positive end tip. Dark red and green surfaces display net positive and negative electron densities, respectively. The free α-helix may be set from the mercapto methylene−polypeptide molecule removing the bridging S atom (Figures 3−6) and then adding a hydrogen atom at the standard bond length. All isovalue surfaces are set at 0.02 (e/Å^3).

the Mulliken and NBO methods gave the same trend, while for others, they gave opposite trends. This fact is evident regardless the type of basis set we used in this work. This type of discrepancy is well-known to occur due to the differences in the partitioning scheme employed in each case.[35] In order to obtain more reliable results, the electrostatic potential at an isodensity values was used as a guide for the changes in the charge distribution of the nanosystem. The electrostatic potential (EP) provides an accurate view of the charge distribution and its changes that is not affected by any partitioning scheme. In this way, the trends found for the different configurations were found without the ambiguities often encountered with the traditional Mulliken and NBO methods.

Results and Discussion

As mentioned above, the results reported in this work are based on calculations using the LanL2MB and 3-21G* pair that we refer to as the nonextended basis set. When explicitly stated, the results using the extended basis set (EBS) are also presented.

The Singlet States: Nonmagnetic States. All quantum singlet states were reached for the α-helix with the up+ and down+ configurations for the two cluster sizes studied. Two steps were considered for the chemisorption process. We studied first the chemisorption of the mercapto-α-polypeptide, starting with a free α-helix in its singlet state and ending at the corresponding nanosystem also at its singlet state. This was done for both configurations of the electric dipole moment. As reference for the EP maps, radical species of both isolated molecular and cluster were also considered (Figures 1b and 2b). These maps help to understand the effects on the charge redistribution during the Au−S covalent bond creation during chemisorption.

In the down+ configuration on the Au_{23} cluster, the EP changes resulting from the chemisorption were tracked by following the changes in color at the top tip methyl group and in the other fragments of the nanosystem. A decrease of electronic charge is evident at the top and midsection of the helix once the thio-α-polypeptide radical is created by the homolitic S−H bond cleavage. A dipole moment depletion of 12.0 D was also observed (Figure 1a,b). When using the EBS, such moment depletion was 10.5 D. EP maps and variations were similar to those shown on Figure 1a,b, but the S atom became less negatively charged; meanwhile, the complementary negative charge remained localized at the top methyl group. Greater NBO charge and dipole moment values made evident a more localized and polarized electron density (caption of Figure 1 and Table 1).

After chemisorption, the S atom at the lower tip (Figure 1c) becomes more negative and the Au cluster becomes more positive (Figures 1b,c). In the middle of the structure, the methylene group (C55 on Figure 3) becomes more negative. At the upper tip of the electric dipole, the methyl group becomes more negative also (Figures 1b,c). This group became even more negatively charged when the EBS was used. Similar EP-EBS maps for both the α-helix at its mercapto and chemisorbed forms (not shown) and the non-EBS map for mercapto of Figure 1a is also shown. Hence, while preserving it, the use of the EBS gives a more moderate version of the already observed trend with the non-EBS that the whole α-helix is more negative with respect to the radical but not as much as in the free molecule (Figure 1a,c). Such a result was consistent with calculated changes in the NBO charge on atoms at both ends of the tips during chemisorption (Table 1). Then, a net charge transfer from the Au_{23} cluster to both the S atom and α-helix was found after the homolitic bond creation (Figures 1b,c). The charge rearrangement associated with α-helix chemical reduction and covalent S−Au bond creation was responsible for the 7.1 D increase for the total dipole moment with respect to the free radical species (Figure 1b,c and Table 1). EBS calculations proved a higher α-helix chemical reduction as responsible of a 12.7 D increment. In Table 1, we see that the α-helix had a negative NBO charge after chemisorption, which is just the opposite of that in the Au cluster. This charge rearrangement is in agreement with that proposed in ref 10 for the *final* step in the charge rearrangement upon chemisorption. We have to mention, that the model of ref 10 refers to macroscopic interfaces and our model contains only one molecule. Clearly, differences may arise from collective and size effects not considered in our simple model. The orientation of the electric dipole proposed in ref 10 before chemisorption is just the opposite to the one found in this work to produce a decrease of the dipole of the

TABLE 1: NBO and Mulliken Charge Distributions at the Given Nanosystems

	total charge (au)[d] NBO Mulliken			
	q_{Au}[a]	q_S[b]	q_α[c]	μ[d,e] (D)
down+ radical		−0.046 (−0.060)	0.046 (0.060)	19.0
		−0.070 (0.740)	0.070 (−0.740)	(22.9)
down+ Au_{23} cluster, singlet state	0.366 (0.453)	−0.353 (−0.396)	−0.013 (−0.060)	26.1
	−0.086 (−0.262)	−0.011 (0.220)	0.097 (0.041)	(35.6)
down+ Au_{23} cluster, magnetic state	0.312 (0.432)	−0.355 (−0.397)	0.043 (−0.034)	22.4
	−0.139 (−0.282)	−0.014 (0.219)	0.152 (0.063)	(34.2)
down+ Au_{55} cluster, singlet state	0.275	−0.348	0.073	21.7
	−0.179	−0.005	0.184	
down+ Au_{55} cluster, magnetic state	0.191	−0.351	0.160	16.2
	−0.261	−0.008	0.269	
up+ radical		0.118 (0.094)	−0.118 (−0.094)	31.2
		0.073 (0.011)	−0.073 (−0.011)	(34.6)
up+ Au_{23} cluster, singlet and magnetic states	0.268 (0.304)	−0.308 (−0.339)	0.040 (0.034)	37.1
	−0.243 (−0.464)	0.067 (0.281)	0.175 (0.183)	(38.9)
up+ Au_{55} cluster, singlet and magnetic states	0.206	−0.271	0.065	37.1
	−0.313	0.102	0.210	

[a] Gold cluster total charge. [b] Sulfur atom total charge. [c] α-Helix total charge. [d] Extended basis set calculation results are in parentheses. [e] Nanosystem dipole moment.

TABLE 2: Some Characteristic Properties of the Au_{23} Cluster Nanosystem

	magnetic state[I]					singlet state:[I]		
conf	$S_{thio\text{-}\alpha}$[a] (au)	$q_{thio\text{-}\alpha(M)}$[b] (au)	$\mu_s(0.0)$[c] $\mu_s(\Delta E_{ss}/2)$[d] (au)	μ_s[d] (au)	ΔE_{ss}[e] (eV)	$q_{thio\text{-}\alpha(S)}$[f] (au)	ΔE[g] (cal/mol)	$\Delta Q_{thio\text{-}\alpha}$[h] (au)
down+	0.20166	−0.311	0.9148	0.9042	−0.487	−0.366	−540.0	0.055
	(0.07325)	(−0.432)	−0.9257	(0.5445)	(−0.200)	(−0.453)	(−72.6)	(0.021)
up+	0.00000	−0.268	0.0000	5.801×10^{-6}	0.000	−0.268	0.00	0.000
			0.0000					

[a] Thio-α-helix Mulliken total spin population. [b] Magnetic state thio-α-helix NBO total charge. [c] Net magnetic moment including spin states up to Fermi level and above up to $\Delta E_{ss}/2$ level. [d] Net magnetic moment calculated from the Gaussian 03M output. [e] Magnetic state energy splitting. [f] Singlet state thio-α-helix NBO total charge. [g] Magnetic state relative stability energy. [h] $\Delta Q_{thio\text{-}\alpha} = q_{thio\text{-}\alpha(M)} - q_{thio\text{-}\alpha(S)}$. [I] Extended basis set calculation results appear in parentheses.

TABLE 3: Some Characteristic Properties of the Au_{55} Cluster Nanosystem

	magnetic state							
conf	$S_{thio\text{-}\alpha}$[a] (au)	$q_{thio\text{-}\alpha(M)}$[b] (au)	$\mu_s(0.0)$[c] $\mu_s(\Delta E_{ss}/2)$[d] (au)	μ_s[d] (au)	ΔE_{ss}[e] (eV)	singlet state: $q_{thio\text{-}\alpha(S)}$[f] (au)	ΔE[g] (cal/mol)	$\Delta Q_{thio\text{-}\alpha}$[h] (au)
down+	0.32464	−0.192	0.9168	1.1987	−0.324	−0.275	−1090	0.083
			−0.4750					
up+	0.00001	−0.206	0.0000	0.0001	0.000	−0.206	0	0.000
			0.0000					

[a] Thio-α-helix Mulliken total spin population. [b] Magnetic state thio-α-helix NBO total charge. [c] Net magnetic moment including spin states up to Fermi level and above up to $\Delta E_{ss}/2$ level. [d] Net magnetic moment calculated from the Gaussian 03M output. [e] Magnetic state energy splitting. [f] Singlet state thio-α-helix NBO total charge. [g] Magnetic state relative stability energy. [h] $\Delta Q_{thio\text{-}\alpha} = q_{thio\text{-}\alpha(M)} - q_{thio\text{-}\alpha(S)}$.

α-helix. We have to recall that the model of ref 10 is entirely classical, and subtle quantum mechanical effects are not considered. A significant discrepancy between such different models should not be then entirely unexpected. It is interesting to mention that the charge transfer from the Au cluster to the adsorbate assumed in ref 10 is indeed observed in our model.

Even though the positive end of the dipole of α-helix (Figure 1a) is oriented toward the Au surface, the EP has a small negative region at the S atom that is reinforced after chemisorption (Table 1). By increasing the Au cluster size, we found that the methyl group of the top of the α-helix becomes more positive (Figure 1c,e), the lower thio tip showed no apparent change, while the Au cluster surface becomes more negative. The larger charge rearrangement at the top of the α-helix seems to be responsible for a dipole moment depletion of 4.4 D (Figure 1c,e). A reduction of total electric charge of the thio-α-helix of 0.1 au was also observed (Tables 3 and 4). As seen in Table 1, the Au cluster showed a rather weak positive potential that becomes less so as the cluster size is increased. Also, we found that the NBO charge of the Au_{55} cluster is less than that of the smaller one, so the Au surface becomes less chemically reductive as the size of the cluster is increased.

For the up+ configuration case, the EP became slightly more positive over the middle and lower regions of the α-helix, while the nanosystem's dipole moment increased by 5.7 (EBS 4.3) D. Such increment may be understood as equivalent to the

TABLE 4: Charge Increment for Thio-α-helix Polypeptide's Top Tip at Magnetic State[a]

atom in Figure *3*	NBO top tip atomic charge changes with respect to the singlet state (au)				
	74 (N)	73 (O)	69 (C)	67 (N)	66 (O)
down+ config Au_{23} cluster	0.006	0.017	−0.006	0.008	0.006
	(0.003)	(0.008)	(1.7×10^{-4})	(0.003)	(0.002)
down+ config Au_{55} cluster	0.008	0.025	−0.001	0.014	0.009

[a] Extended basis set calculation results are in parentheses.

chemisorption dipole moment provided other electron density effects may also be considered. Smaller variations on the dipole moment as well as on the EP map during chemisorption are indicative of a more closer to rigid electron density,with respect to nuclei positions, than the one found for the down+ configuration. A net charge transfer to the Au_{23} cluster was apparent, coming from the α-polypeptide during the bond formation (Figure 2a−c).

Since no significant change was seen in the EP map at the top of the α-helix, then it seems that the net change on the dipole moment was a consequence of the S−Au bond formation. The trend to positive values becomes accentuated as the cluster size was increased and the S atom becames less negatively charged (Figure 2c,d). The dipole moment remains practically constant (37 D) when the size of the Au cluster was increased, while a depletion of the α-helix electric charge of 0.06 au (Tables 2 and 3) was observed. Then, the small changes observed in the EP around the S atom seemed to contribute little to the variation of the dipole moment of the nanosystem. The variations in the EP map for the different cluster showed that an increase in the number of Au atoms renders them less reductive (Table 1).

Additionally, we observed that the EP of the Au cluster depended on the effective oxidative strength of the S atom, which in turn depended on what peptide end was connected to the thio methylene group. Thus, if the S atom is embedded into a positive EP region, it tends to increase its oxidative strength (Figures 1a and 2a and NBO charge entries in Table 1).

We found that the DOS results were quite dependent on the size of the Au cluster. DOS plots for the different surfaces were built for the same quantum states (Figures 10 and 11). In the DOS spectra derived from the down+ configuration, it was found that there were no holes next to the Fermi level. On the contrary, for the up+ configuration case, holes were found there (the biggest one centered at 0.6 eV showing an energy gap of 0.7 eV).

From Figures 10 and 11, we see that, above 1.0 eV, many DOS minima tend to disappear due a curve smoothing effect while passing from the small to the big cluster. This is as a result of the increase in the total number of states as the size of the cluster is also augmented. For the up+ configuration, we found that the width of the hole (now centered at 0.4 eV) inside the same energy interval is reduced by about 28% upon cluster increase.

Down+ Configuration and the Au_{23} Cluster: The Magnetic State. For the down+ configuration in the Au_{23} cluster, the magnetic state energy is 540 (EBS 73) cal/mol more stable than the singlet state (Table 2). We see that the improved accuracy of EBS reduces the energy difference but still preserves a favorable tendency toward the magnetic state which is greater than the one of ∼16 cal/mol reported by Gonzales et al.[1] for the same EBS. This relative stabilization was caused by the breaking of symmetry in the eigenvalue spectrum, splitting α-

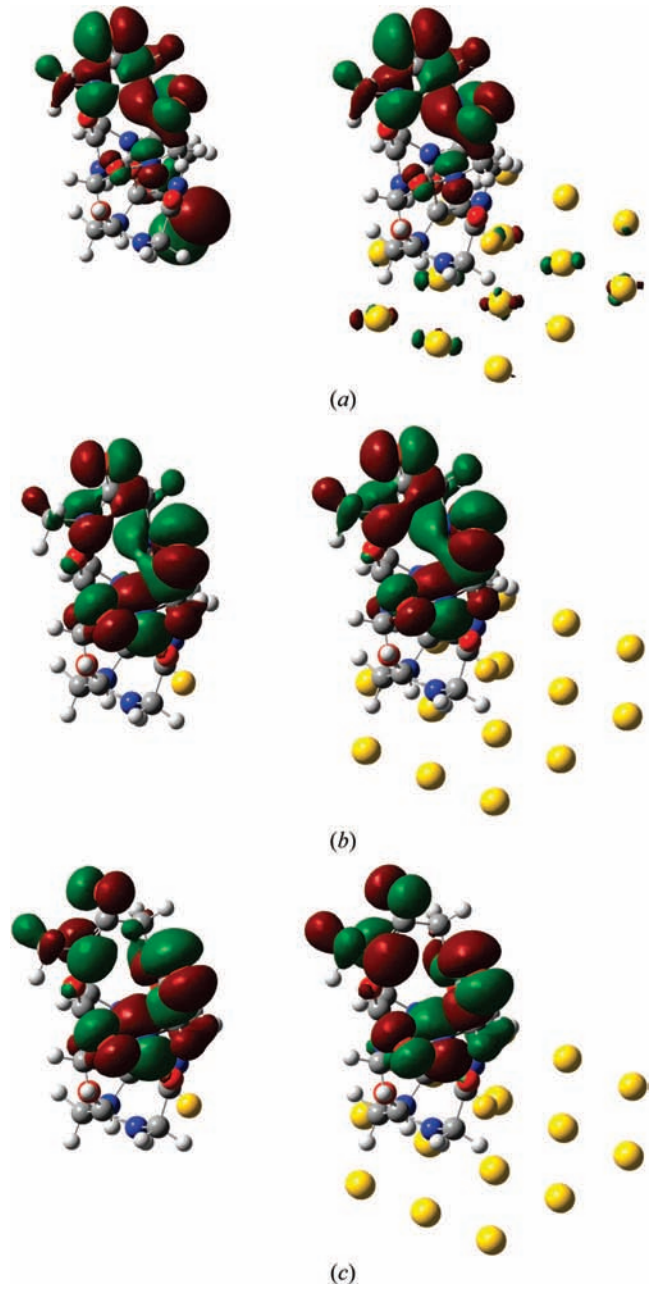

Figure 8. Magnetic orbital as viewed from the top: (left) thio-α-helix radical, (right) down+ conformation on the Au_{23} cluster. (a) SOMO orbital β. (b) SOMO orbital α. (c) SOMO orbital $\beta-1$. All isovalue surfaces are set at 0.02 (e/Å^3). Dark red and green surfaces display net positive and negative electron densities, respectively.

from β-electrons with a moderate energy value close to 0.5 (EBS 0.2) eV or 11.23 kcal/mol (Figure 9a, Table 2). Such symmetry breaking is accompanied by an important charge rearrangement in the nanosystem. Changes to positive EP values were found at the top tip methyl group (Figure 1c,d), while for the α-helix's top and midsection the EP values were quite similar to that of the radical species (Figure 1b,d) but shifted to more positive values. Additionally, no appreciable changes wee seen in the EP at the lower thio-α-helix's tip while the Au cluster changed to more negative values. These variations in the EP maps were reflected in the Mulliken and NBO charge changes of the nanosystem, as seen in Tables 1, 3, 4, and 5. The use of EBS systematically causes smaller variations on the EP maps. The EP map for α-helix in Figure 1c resembled the EP map for the EBS-magnetic state (not shown). On the other hand, the EP

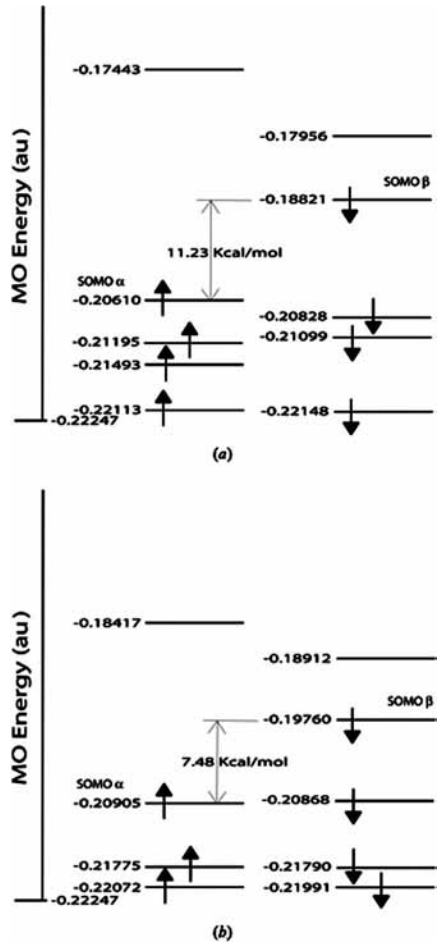

Figure 9. (a) Eigenvalue spectrum as seen near Fermi level (set at SOMO β) for the down+ conformation on the Au_{23} cluster at its magnetic state. (b) Ditto on the Au_{55} cluster.

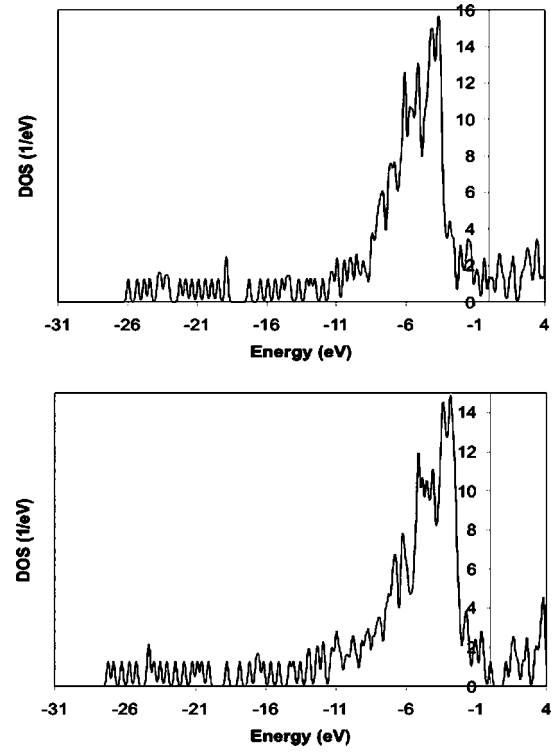

Figure 10. Total DOS for the Au_{23} at its singlet nonmagnetic state, evaluated as the addition of the α and β spin densities (α SDOS + β SDOS). The top−bottom sequence shows plots for the nanosystem's down+ and up+ configurations. This up+ singlet DOS has the same appearance as the corresponding DOS plots for the up+ magnetic state (not shown). The Fermi level is set at the origin of the energy axis scale.

map for the mercapto in Figure 1a resembled the EP map for the EBS-singlet state (not shown). Thus, we conclude that the EP maps for the chemisorbed substrate trend to look like EP maps of its free mercapto derivative.

A dipole moment reduction of 3.7 (EBS 1.4) D accompanied by an electric charge reduction of 0.06 (EBS 0.02) au at the thio-α-helix molecule (Tables 1 and 2) was found. Since passing from the singlet state to the magnetic one does not involve S−Au bond formation, we asume that such dipole moment reduction was a consequence of the charge redistribution and transfer from α-helix to the Au cluster. We can roughly estimate the magnitude of the dipole moment involved in S−Au bond if we consider that in its formation there is not appreciable charge rearrangement at the α-helix fragment. Thus, passing from state b to state d in Figure 1 involves just the S−Au bond formation; i.e., the radical species keeps its chemical properties during the homolitic formation of the S−Au covalent bond. A value of 3.5 (EBS 2.2) D was found, being smaller than that for the up+ configuration and having an inverted sign (5.7 D). Since organic fragment EP maps of mercapto-α-helix and down+ nanosystem were too similar, we took the first one as reference for doing this estimation by adding the $\mu_{EBS} = 0.1$ D value for the Au_{23} cluster.

The charge of atoms at the α-helix's top becomes slightly more positive with respect to the singlet state after chemisorption with variations raging from 0.006 to 0.017 au (EBS from 1.7 $\times 10^{-4}$ to 0.008) (Figures 1c,d and 3 and Table 4). These results are in excellent agreement with the experimental trends obtained by Carmeli et al.[9] The predicted trend toward a more stable magnetic state where the organic molecule exhibits reduced dipole moment as a result of the charge transfer from the molecule to the Au cluster seems to be confirmed by our calculations[6,9] in a rather simple model. Nevertheless, we have to mention that, in our case, the reduction in dipole moment is caused by the high polarizability of the helix produced by the large number of states found near the Fermi level [mainly excited states laying just above it causing no holes in DOS spectra (see Figures 10a and 12a)]. In the case of the macroscopic system, it was assumed that due to the low polarizability of the organic molecules employed, the charge transfer with the metallic surface was the cause of the reduction of the dipole moment.[10] In our simple model, the charge transfer from the Au cluster to the helix seemed to stabilize the high polarizabily state as seen in Figure 1d.

At the magnetic state, we found that the frontier orbitals defining the energy splitting (SOMO α and SOMO β) (Figure 8a,b) were antisymmetric: the signs of the α-helix's top lobe of SOMO α were the complementary ones of SOMO β's, particularly those localized on atoms 66, 67, and 73 (O, N, and O in Figures 1 and 3). Having similar shapes, the SOMO α and SOMO β exhibit different lobe sizes and orientations with respect to their atom sites. Small SOMO α−SOMO β overlaps, either positive or negative, were expected, so regions with nonzero overlap will be those where there is rather appreciable magnetism. This lobe mismatch was much more noticeable at the N and O sites of the tip of the α-helix.[27] If we consider the SOMO $\beta-1$ orbital (Figure 8c), we see that it showed that the overlap with the SOMO α orbital is less than with the β one, thus generating an additional contribution to the magnetism of

TABLE 5: Charge Increment for Thio-α-helix Polypeptide's Lower Tip at Magnetic State[a]

	NBO low tip atomic charge changes with respect to the singlet state (au)				
atom in Figure *3*	32 (N)	31 (O)	27 (C)	25 (N)	79 (O)
down+ config Au_{23} cluster	2.0×10^{-5} (1.0×10^{-4})	−0.002 (-7.7×10^{-4})	2.0×10^{-5} (0.0)	1.5×10^{-4} (2.0×10^{-5})	−0.002 (−0.001)
down+ config Au_{55} cluster	5.0×10^{-5}	−0.002	8.0×10^{-5}	1.7×10^{-4}	−0.003

[a] Extended basis set calculation results are in parentheses.

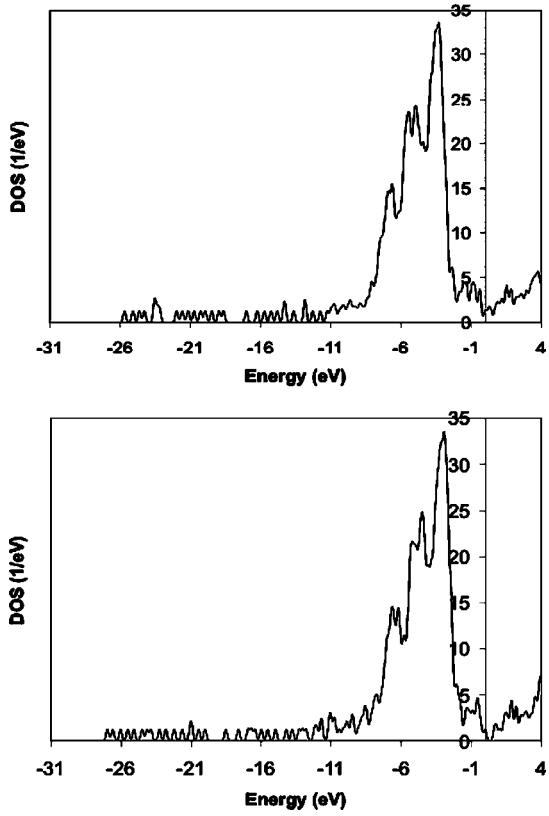

Figure 11. Total DOS for the Au_{55} cluster at its singlet nonmagnetic state, evaluated as (α SDOS + β SDOS). The top−bottom sequence shows plots for the down+ and up+ configurations. This up+ singlet DOS has the same appearance as the corresponding DOS plots for the up+ magnetic state (not shown). The Fermi level is set at the origin of the energy axis scale.

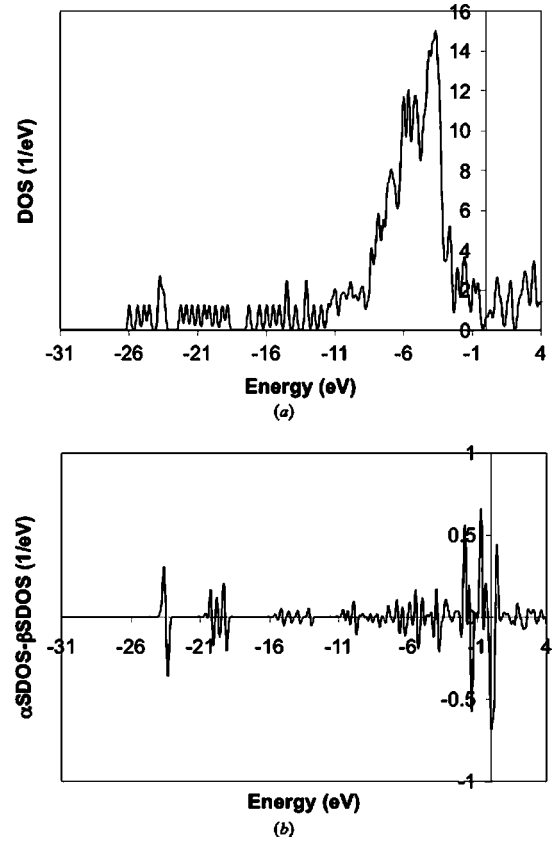

Figure 12. Down+ configurations plots: (a) Total DOS for the Au_{23} nanosystem at its magnetic state and (b) difference between the spin densities α SDOS − β SDOS. The Fermi level has been set at the origin of the energy axis scale.

the nanosystem in atoms 73, 66, and 74. For lower energy orbitals, similar contributions were also found. The presented analysis applies to both magnetic states: the one of the chemisorbed α-helix and that of the free radical since the SOMO α and SOMO β orbitals exhibited rather similar special distributions (see Figure 8). The SOMO α and SOMO β orbitals were quite close in energy, and the resulting energy splitting ΔE_{ss} was 11.23 (EBS 4.61) kcal/mol for the nanosystem (Figure 9a) and 12.55 (EBS 12.32) kcal/mol for the radical.

According to our results, a more stable magnetic state for the nanosystem reflects the Hund's rule[36] of spin multiplicty. The spin isodensity plots for this magnetic state at the 5.0×10^{-3} au isovalue are shown in Figure 4b. The α spin isodensity was mainly localized at atoms 66, 67, and 73 and may be associated with a ferromagnetic state. A NPA study showed that the origin of magnetism was the asymmetry in the population of the 2p orbitals (Table 8). From Table 8, we found that the NPA populations were quite similar to the Mulliken spin density for all the atoms, so we used the latter in our study. At lower isovalues, the isodensity surface showed that the spin α was localized at the top of the α-helix and spin β was, instead, localized in the Au cluster. This is a feature that characterizes an antiferromagnetic state. A comparison of the signs of the different parts of the nanosystem shows that, at the 4.0×10^{-4}au isovalue, the spin isodensity at the α-helix had a sign that is opposite to that found in the Au atoms of the surface (Figure 5b).

From Figures 4 and 5, we note the quite similar spatial spin distributions for the chemisorbed α-helix and its free radical. The radical downward α spin density is canceled by β density excess at the metallic cluster (Figure 5a,b) localized at the SOMO β orbital and those above the Fermi level (Figures 9a, 12b, and 13a). This picture is reinforced with the idea of creating a chemical bond by pairing opposed spin electrons or direct exchange interaction. The short-lived radical quantum state is frozen somehow and some of its properties are preserved by the α-helix chemisorption (also compare α-helixes in Figure 1b,d). The use EBS translates into halved ΔE_{ss} value for the frozen radical, again a quantitative variation that does not modify the qualitative stability trend observed for the smaller basis set.

We found that the electronic structure of adsorbate is varying upon chemisorption as Naaman et al. did for dense assembled packed layers.[10] It is important to notice that the polypeptide

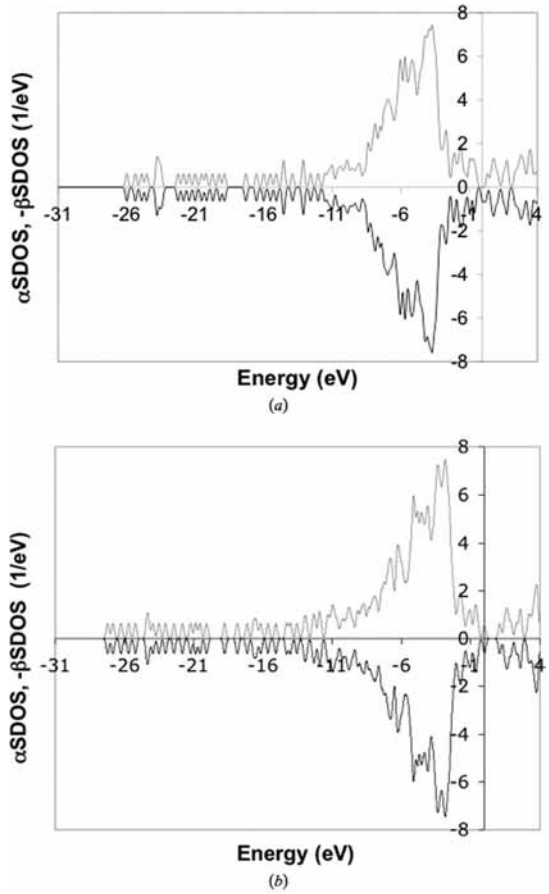

Figure 13. Down+ configurations plots: (a) Superimposed α (positive valued) and β (negative valued) spin SDOS densities. Up+ configuration plot: (b) Superimposed α (positive valued) and β (negative valued) spin SDOS densities for the Au_{23} cluster nanosystem at its singlet or magnetic states. (S)DOS show the chemisorption-induced asymmetries just for the down+ configuration. The Fermi level has been set at the origin of the energy axis scale.

LUMO molecular orbital at its positive terminal (Figure 7c) is closer to the metallic surface and is allowed to interact with it through the S bridge atom (see Figure 4b), facilitating the excited states stabilization by coupling between metal and molecular orbitals, as suggested by Vondrak et al.[37] These observations were consistent with the previous result about the similarity in the α-helix and the radical of the SOMO α and β orbitals (Figure 8). The magnetic moment for the down+ configuration on the Au_{23} cluster was approximately half (EBS one-fourth) of that of the free radical (Table 2) and is found in the range reported by Ichii et al. for alkanethiol self-assembled monolayers. This difference may due to the presence of uncanceled radical α spin density at the top of the chemisorbed α-helix (Figures 4a,b and 5a,b). For the EBS case, such α spin density cancelation is reinforced with the greater charge transfer from the Au_{23} cluster acting as a chemically more reductive agent. The stable spin localization found for the down+ configuration might be equivalent to a qubit in quantum information processing.[38] After studying the EBS results, we noted that all qualitative nanosystem features descriptions given for the analysis of non-EBS results are applicable to the EBS case, except for the absolute magnitude of the electric and magnetic properties, where a variation of one-half to one-third is observed.

From the total DOS spectra of the magnetic state, we found that a hole next to the Fermi level at −0.1 eV (Figure 12a) existed. The DOS at this energy showed a lowering of 0.7 eV^{-1} when compared to the singlet state. Such result may be attributed to a downward shift, in the energy scale, of the majority-spin (α) states. The existence of the hole near the Fermi level seems to indicate that less conductor character is expected for the adsorbed surface in its magnetic state. This showed a relation between the net magnetization and the holes of the DOS below the Fermi level [Figures 10 (top) and 12a].[1] The eigenvalue energy level shift was also evident in Figures 12b and 13a, where a certain degree of SDOS asymmetry was observed around the Fermi level. Additionally, from Table 2 it is apparent that the Au_{23} nanosystem magnetic moment μ_s showed high sensitivity toward the way in which the summation of the magnetic spin states was done, since the values of $\mu_s(0.0)$ and $\mu_s(\Delta E_{ss}/2)$ were very close in magnitude while the inverted sign was found. Such inversion may be a consequence of our somewhat arbitrary definition of the position of Fermi level for the extended system.

TABLE 6: Charge and Spin Variations with Au Cluster Size[a]

atom in Figure 3	NBO atomic charge and spin changes as metallic cluster size is increased at the magnetic state (au)				
	74 (N)	73 (O)	69 (C)	67 (N)	66 (O)
spin	0.01480	0.03561	0.00126	0.03183	0.01865
charge	0.010	0.022	−0.002	0.015	0.013

[a] Nonextended basis set calculation results.

TABLE 7: Energy Gaps on the Studied Nanosystems[a]

config	HOMO−LUMO energy gap (kcal/mol)	
	Au_{23}	Au_{55}
down+	5.42	5.26
up+	25.33	15.09

[a] Nonextended basis set calculation results.

Down+ Configuration and the Au_{55} Cluster. For the down+ configuration of the α-helix in the Au_{55} cluster, a 34% increase in the charge transfer from the helix to the Au cluster was accompanied with a decrease of 5.5 D for its dipole moment (Table 1). For the larger cluster, the EP map at the tip of the helix showed a smaller change than in the Au_{23} cluster.

The final magnetic state on the Au_{55} cluster exhibited an energy that is 1090 cal/mol more stable compared to the singlet nonmagnetic state (Table 3). The stabilization energy caused by the breaking of symmetry showed a smaller value of 0.31 eV or 7.48 kcal/mol (Figure 9b) than in the smaller cluster. The ferromagnetic state effect, the α spin isodensity localized at atoms 66, 67, and 73, had the same appearance as in the Au_{23} (Figure 4b,c). The volumes in the isospin densities for the Au_{55} cluster were twice the one found for the smaller cluster. The isospin density surfaces found at the α-helix's top were very similar to those found in the Au_{23} cluster (Figures 4c and 5c). Also, frozen radical state properties seem to be preserved (Figures 4a,c) and even some state characteristics seem to be restored, like the case of the α spin density at the S atom (Figures 5a,c). The increase in the metallic surface size when passing from Au_{23} to Au_{55} produced a favorable energy difference ΔE of −500 cal/mol (Tables 2 and 3). Since this estimation was made using non-EBS, such stabilization energy value is questionable due to its poor accuracy. However, the existence of a relatively stable magnetic state regardless the Au cluster size is remarkable. Both α-helix's Mulliken total spin density and NBO electric charge increased in about 0.1 au (Tables 2 and 3). Most of the atoms at the α-helix's top became

TABLE 8: Au_{23}-Nanosystem: NBO α and β Population Analysis for the Given Atoms

atom in Figure *3*	orbital analysis per atom majority-spin α [minority-spin β] $\mu_{S\text{-}NPA}$[a] (spa)			total population	Mulliken spin density (spa)[b]
	2s	2p			
O	0.85	2.43		4.28193	0.028272
(66)	[0.85]	[2.41]		[4.25465]	(0.007642)
	0.00	0.02		0.02728	
	2s	2p			
N	0.64	2.23		3.86693	0.063492
(67)	[0.64]	[2.17]		[3.80822]	(0.019864)
	0.00	0.06		0.05871	
	2s	2p			
O	0.85	2.46		4.30946	0.088906
(73)	[0.85]	[2.37]		[4.22202]	(0.035348)
	0.00	0.09		0.08926	
	2s	2p			
N	0.64	2.21		3.843139	0.032733
(74)	[0.63]	[2.18]		[3.814390]	(0.015494)
	0.01	0.03		0.028749	
	6s	5d	6p		
Au	0.425 52	4.88601	0.04047	39.35122	−0.002497
(closest to S atom)	[0.42612]	[4.88910]	[0.04045]	[39.35489]	(−0.001501)
	−0.00060	−0.00309	0.00002	−0.00367	

[a] α, β spin density difference given in units of spin per atom (spa). [b] Extended basis set calculation results are in parentheses.

more positive in the larger cluster than the Au_{23} system (Figure 3 and Table 6).

We found that, at the present calculation level, a net electronic charge transfer from the α-helix toward the Au cluster surface occurred when the magnetic state was reached (Figure 1e,f). However, by considering the whole absorption process on the small Au cluster (Figure 1a,d) we could note how Au atoms released a greater amount of electron charge to the α-helix that was stored, in part, at the S atom, allowing almost identical EP maps for both α-helix species at states b and d. Once more, the resulting charge rearrangement was consistent with that in ref 19. These experimental results showed that, for Au surfaces covered with layers of molecules having electropositive end groups, a net electron charge transfer from the metallic substrate was observed. Such molecules can store the excess of charge in their carboxyl groups.[19] By analogy, the methyl group at C 76 in the α-helix may be taken as the electropositive end group and the S atom bonded to the Au cluster corresponds to the charge storing molecular fragment of ref 19. Since the S atom is next to the adsorbate−substrate interphase, we think that it contributes to its electronic density.

In the large cluster, we again found that the way in which we did the summation of net magnetic spin states influenced the results. The $\mu_s(0.0)$ value remained closed to the value obtained for the previous case of small clustered-nanosystem; however a 50% magnitude depletion and inversion were found for $\mu_s(\Delta E_{ss}/2)$ (Table 2).

If one takes the results of $\langle S^2 \rangle$ obtained with Gaussian, the magnetism increases with the size of the cluster (Tables 2 and 3). This result is valid only for the nanosystems and just reflects their total spin density (Figures 4b,c). If we consider the values obtained with the method that includes DOS information, we indeed note that they model an extended system. Clearly, the results for the larger Au cluster will represent much better a macroscopic system than those obtained for the smaller cluster. We consider negative values for $\mu_s(\Delta E_{ss}/2)$ as a model feature for the decreasing trend on μ_s with cluster size. Our predicted μ_s values, close to 0.9 au for clustered systems (Tables 2 and 3) lay inside the range reported by Ichii et al.[4] for similar type of adsorbate. We expect, for our extended systems, such values to be smaller and even to invert their signs. This was confirmed by the calculated values for the larger cluster that showed that the magnetism decreases with size, as found experimentally in Fe clusters.[39]

Up+ Configuration. All studied magnetic states for this configuration (both cluster sizes) were found to be energetically degenerated with respect to the singlet state showing the same total DOS spectra (Figures 1b and 2b) and practically having the same electric dipole moment. As for the down+ configuration, the net NBO electric charge increased about 0.06 au (Tables 2 and 3) and the α-helix's total spin density increased about 10 times (scale ratio for which both isospin surfaces approximately encompassed the same volume) by increasing the cluster size. The magnetic moment and the α-helix's spin density, mainly localized at the bonded S atom, are significantly less than those found for the down+ configuration (compare Tables 2 and 3, Figures 5b,c and 6b,c). This was corroborated by the presence of a hole near 1.0 eV away from the Fermi level in the total DOS spectrum (Figures 1 and 2) even though no appreciable symmetry breaking in the SDOS plots was visible (Figure 13b).

The magnetization found in systems with the up+ configuration was very small, since a tiny spin symmetry breaking region (involving α and β molecular orbitals that are nearly degenerated) leads to very small magnetic band splitting values. The small variations observed for the magnetic properties are as a consequence of the rigid-fixed-to-nuclei character of the electron density for the up+ configuration.

In general, passing from a singlet state to a broken-spin-symmetry magnetic state does not involve a significant energy change of the nanosystem nor an important rearrangement of its charge distribution between the metallic surface and the adsorbate (Figure 2c,d). Thus, upon chemisorption, no significant variation in electronic structure of the adsorbate was observed. The latter statement was confirmed by an almost constant dipole moment found when the Au cluster size was changed. After using EBS we saw that the whole qualitative description given so far for the up+ configuration results also apply to this

approximation level. So a smaller magnetic moment for up+ configuration with respect to the down+ one should be expected for small Au clusters with a single polypeptide molecule on it. The origin of magnetism for this configuration can be explained on the basis of the treatment introduced thoroughly by Gonzalez et al.[1]

Conclusions

The use of the wave function BS-UDFT method for representing the magnetic states due to the chemisorption of an α-helix on Au clusters proved to be satisfactory in estimating the magnetic and electric properties. According to the nanosystem size, we used two basis sets, which offer different approximation levels and accuracies. The use of non-EBS gives a qualitative character to the analyses of magnetism upon chemisorption and also gives a valuable insight on the relation between charge transfer, electron density, and spin density variations with respect to gas phase values. Using the EBS adds some predictive character on the electric and magnetic properties but does not change the trends established with the smaller basis set. The persistence of the relative stable magnetic state using the more accurate calculation gives a much firmer basis for the validity of our analysis. By doing the comparison of electric and magnetic properties obtained from approximation levels, an almost constant scaling factor of between $^1/_2$ and $^1/_3$ is observed.

We have found that the orientation of the electric dipole of the α-helix was determinant in the formation of magnetic domains. For up+ configurations, for which EP maps showed a close to rigid[40] electron density with respect to nuclei positions, the chemisorption did not produce significant modification of the electronic structure of adsorbate. Only a small charge transfer mostly localized at the S−Au bond and a slight increase in the resulting electric dipole moment were produced. This localized transfer produced a very small magnetization for these configurations. In down+ configurations, with nonrigid electron densities, where a more delocalized transfer was found, a much higher magnetization was obtained and adsorbate electronic structure variations were observed. This fact gives further support to the idea that the charge transfer process associated with a reduction of the electric dipole moment determines the magnetism in these nanosystems.

The localization of molecular spin induced by the chemisorption process opens up the intriguing possibility of using similar systems in a quantum information processing devices.[38]

There is a clear correlation between the DOS profile in the neighborhood of the Fermi energy in the singlet nonmagnetic state and the onset of the symmetry breaking associated with the magnetic state. This correlation is evident from the comparison between Figures 8 and 9, on one side, and 10, on the other: The DOS around the Fermi energy for the precursor singlet state in the up+ configuration exhibits a gap, whereas for the down+ configuration the corresponding DOS is gapless. In other words, the precursor state for the magnetic (nonmagnetic) state is more metal-like (semiconductor-like). This is an interesting result insofar it allows us to establish a connection with the Stoner criterion in the theory of itinerant magnetism in metals, which requires a nonvanishing DOS at the Fermi energy.

It is important to notice that for the down+ configurations, the polypeptide SOMO β molecular orbital at its positive terminus is closer to the metallic surface and is allowed to interact with it through the S bridge atom, facilitating the excited states stabilization by the coupling between metal and molecular orbitals.[37] Such stabilization could lead to properties that are characteristic of radical species: frozen radicals. The system is then found in such a magnetic state where electron density is delocalized into the thio-α-helix adsorbed on the Au cluster.[41] Under this configuration, the more stable magnetic state is nearly degenerated with the singlet state and the degree of degeneration increases with the basis set size.

We found that an increase in the cluster size produced a decrease in the magnetic moment. Our calculations showed two important features that follow the same trend reported by Naaman et al.:[5−10] the reduction of the thiopolypeptide electric dipole moment and the charge transfer between the metallic surface and the chemisorbed molecule. Although the magnitudes for the spin density and magnetic moments may seem rather small when compared with those observed experimentally, it is expected that a reinforcing effect by lateral interactions will be present when the formation of a thiopolypeptide monolayer on a macroscopic Au surface takes place. Finally, we found that the increase of cluster size in any magnetic state favored localized α-helix's total spin densities.

Acknowledgment. This work has been supported partially by OPSU, Alma Mater Project, Venezuela. Also, the authors thank Dr. B. Gómez for supplying his Fortran77 code that allowed performing the (S)DOS calculations presented in this work.

References and Notes

(1) Gonzalez, C.; Simón-Manso, Y.; Marquez, M.; Mujica, V. *J. Phys. Chem. B* **2006**, *110*, 687, and references therein.

(2) Zeller R. *NIC Series*, Vol. 31, ISBN 3−00−017350, pp 419−445, 2006 and references therein.

(3) Crespo, P.; Litrán, R.; Rojas, T. C.; Multigner, M.; de la Fuente, J. M.; Sánchez-López, J. C.; García, M. A.; Hernando, A.; Penadés, S.; Fernández, A. *Phys. Rev. Lett.* **2004**, *93*, 087204.

(4) Ichii, T.; Fukuma, T.; Kobayashi, K.; Yamada, H.; Matsushige, K. *Appl. Surf. Sci.* **2003**, *210*, 99–104.

(5) Vager, Z.; Carmeli, I.; Leitus, G.; Reich, S.; Naaman, R. *J. Phys. Chem. Solids* **2004**, *65*, 713–717.

(6) Carmeli, I.; Skakalova, V.; Naaman, R.; Vager, Z. *Angew. Chem. Int. Ed.* **2002**, *41*, 761.

(7) Vager, Z.; Naaman, R. *Phys. Rev. Lett.* **2004**, *92*, 087205–1.

(8) Carmeli, I.; Leitus, G.; Naaman, R.; Reich, S.; Vager, Z. *Israel J. Chem.* **2003**, *43*, 399–403.

(9) Carmeli, I.; Gefen, Z.; Vager, Z.; Naaman, R. *Phys. Rev. B* **2003**, *68*, 115418.

(10) Naaman, R.; Vager, Z. *Phys. Chem. Chem. Phys.* **2006**, *8*, 2217–2224.

(11) Baik, M. H.; Gherman, B.; Friesner, R.; Lippard, S. *J. Am. Chem. Soc.* **2002**, *124*, 14608.

(12) Noodleman, L.; Peng, C.; Case, D.; Mouesca, J. *Coord. Chem. Rev.* **1995**, *144*, 199.

(13) Zhao, X.; Richardson, W.; Chen, J.; Li, J.; Noodleman, L. *Inorg. Chem.* **1997**, *36*, 1198.

(14) Ruiz, E.; Cano, J.; Alvares, S.; Alemany, P. *J. Comput. Chem.* **1999**, *20*, 1391–1400.

(15) Isobe, H.; Soda, T.; Kitagawa, Y.; Takano, Y.; Kawakami, T.; Yoshioka, Y.; Yamaguchi, K. *Int. J. Quantum Chem.* **2001**, *85*, 34.

(16) Shenker, R.; Mandimutsira, B.; Riordan, Ch.; Brunold, T. *J. Am. Chem. Soc.* **2002**, *124*, 13842.

(17) Takano, Y.; Kubo, S.; Onishi, T.; Isobe, H.; Yoshioka, Y.; Yamaguchi, K. *Chem. Phys. Lett.* **2001**, *335*, 395–403.

(18) Gottschalck, J.; Hammer, B. *J. Chem. Phys.* **2002**, *116*, 784.

(19) Ray, S.; Cohen, H.; Naaman, R.; Liu, H.; Waldeck, H. *J. Phys. Chem. B* **2005**, *109*, 14064.

(20) Mujica, V.; Nieto, P.; Puerta, L.; Acevedo, S. *Energy Fuels* **2000**, *14*, 632–639.

(21) Puerta L.; Franco H.; Mujica V. *Study of the Interaction Between a High Dipolar Moment Thio-polypeptide and a Gold Surface. XXXI Congreso Internacional de Químicos Teóricos de Expresión Latina QUITEL*; Isla de Margarita, Venezuela, 2005, and references therein.

(22) Frisch, M. J. ; Trucks, G. W.; Schlegel, H. B.; Scuseria, G. E.; Robb, M. A.; Cheeseman, J. R.; Montgomery, J. A., Jr.; Vreven, T.; Kudin, K. N.; Burant, J. C.; Millam, J. M.; Iyengar, S. S.; Tomasi, J.; Barone, V.; Mennucci, B.; Cossi, M.; Scalmani, G.; Rega, N.; Petersson, G. A.;

Nakatsuji, H.; Hada, M.; Ehara, M.; Toyota, K.; Fukuda, R.; Hasegawa, J.; Ishida, M.; Nakajima, T.; Honda, Y.; Kitao, O.; Nakai, H.; Klene, M.; Li, X.; Knox, J. E.; Hratchian, H. P.; Cross, J. B.; Bakken, V.; Adamo, C.; Jaramillo, J.; Gomperts, R.; Stratmann, R. E.; Yazyev, O.; Austin, A. J.; Cammi, R.; Pomelli, C.; Ochterski, J. W.; Ayala, P. Y.; Morokuma, K.; Voth, G. A.; Salvador, P.; Dannenberg, J. J.; Zakrzewski, V. G.; Dapprich, S.; Daniels, A. D.; Strain, M. C.; Farkas, O.; Malick, D. K.; Rabuck, A. D.; Raghavachari, K.; Foresman, J. B.; Ortiz, J. V.; Cui, Q.; Baboul, A. G.; Clifford, S.; Cioslowski, J.; Stefanov, B. B.; Liu, G.; Liashenko, A.; Piskorz, P.; Komaromi, I.; Martin, R. L.; Fox, D. J.; Keith, T.; Al-Laham, M. A.; Peng, C. Y.; Nanayakkara, A.; Challacombe, M.; Gill, P. M. W.; Johnson, B.; Chen, W.; Wong, M. W.; Gonzalez, C.; Pople, J. A. *Gaussian 03M, Revision B.04*; Gaussian, Inc., Wallingford, CT, 2004.

(23) Grafenstein, J.; Kraka, E.; Filatov, M.; Cremer, D. *Int. J. Mol. Sci.* **2002**, *3*, 360–394.

(24) Crawford, T. D.; Kraka, E.; Stanton, J. F.; Cremer, D. *J. Chem. Phys.* **2001**, *114*, 24.

(25) Postnikov, A.; Brüger, M.; Schnack, J. http://arxiv.org/PS_cache/cond-mat/pdf/0404/0404343v1.pdf, 2002, pp 1−15.

(26) Dennington, R., II.; Keith, T.; Millam, J.; Eppinnett, K.; Hovell, W. L.; Gilliland, R. *GaussViewM 3.0.9*; Semichem, Inc.: Shawnee Mission, KS, 2003.

(27) Bencini, A.; Carbonera, Ch.; Dei, A.; Vaz, M. *Dalton* **2003**, (9), 1701.

(28) Castro, M. *Int. J. Quantum Chem.* **1996**, *64*, 223–230.

(29) Constantinides, C. P.; Koutentis, P. A.; Schatz, J. *J. Am. Chem. Soc.* **2004**, *126*, 16232–16241.

(30) Press, W. H.; Flannery, B. P.; Teukolsky, S. A.; Vetterling, W. T. *Numerical Recipes: The Art of Scientific Computing*; Cambridge University Press: Cambridge, 1990.

(31) Gomez, B.; Martinez-Magadan, J. *J. Phys. Chem. B* **2005**, *109*, 14868–14875.

(32) Hoffmann R. *Solids and Surfaces: A Chemist's View on Bonding in Extended Structures*; VCH Publishers Inc.: New York, 1988; p 15.

(33) Wang, S.; Yu, J.; Mizuseki, H.; Yan, J.; Wang, C. *J. Chem. Phys.* **2004**, *120*, 8463.

(34) García-Cruz, L.; Baquero, R. *Rev. Méx. Fís.* **2003**, *49*, 317.

(35) Gillespi, R.; Popelier, P. L. A. *Chemical Bonding and Molecular Geometry from Lewis to Electron Densities*; Oxford University Press: New York, 2001; p 153.

(36) Kinoshita, M. *Jpn. J. Appl. Phys.* **1994**, *33*, 5718–5733.

(37) Vondrak, T.; Cramer, C.; Zhu, X. *J. Phys. Chem. B* **1999**, *103*, 8915.

(38) Tamulis, A.; Tsifrinovich, V. I.; Tretiak, S.; Berman, G. P.; Allara, D. L. *Chem. Phys. Lett.* **2007**, *436*, 1–3, 144.

(39) Bansmann, J.; Baker, S.; Binns, C.; Blackman, J.; Bucher, J.; Dorantes-Dávila, J.; Dupuis, V.; Fabre, L.; Kechrakos, D.; Kleibert, A.; Meiwes-Broer, K.; Pastor, G.; Perez, A.; Toulemonde, O.; Trohidou, K.; Tuaillon, J.; Xie, Y. *Surf. Sci. Rep.* **2005**, *56*, 189.

(40) Deutsch, D.; Natan, A.; Shapira, Y.; Kronik, L. *J. Am. Chem. Soc.* **2007**, *129* (10), 2989–2997.

(41) Neuman, O.; Naaman, R. *J. Phys. Chem. B* **2006**, *110* (11), 5163–5165.

JP710748H